Annals of Biomedical Engineering, Vol. 33, No. 4, April 2005 (© 2005) pp. 415–428
DOI: 10.1007/s10439-005-2495-2

Fundamental Study of Ultrasonic-Measurement-Integrated Simulation of Real Blood Flow in the Aorta

KENICHI FUNAMOTO,[1] TOSHIYUKI HAYASE,[2] ATSUSHI SHIRAI,[2] YOSHIFUMI SAIJO,[3] and TOMOYUKI YAMBE[3]

[1]Graduate School of Engineering, Tohoku University, 6-6-01 Aaramaki-Aoba, Aoba-ku, Sendai 980-8579, Japan; [2]Institute of Fluid Science, Tohoku University, 2-1-1 Katahira, Aoba-ku, 6-6-01 Sendai 980-8577, Japan; and [3]Institute of Development, Aging and Cancer, Tohoku University, 4-1 Seiryomachi, Aoba-ku, Sendai 980-8575, Japan

(Received 4 June 2004; accepted 6 October 2004)

Abstract—Acquisition of detailed information on the velocity and pressure fields of the blood flow is essential to achieve accurate diagnosis or treatment for serious circulatory diseases such as aortic aneurysms. A possible way to obtain such information is integration of numerical simulation and color Doppler ultrasonography in the framework of a flow observer. This methodology, namely, *Ultrasonic-Measurement-Integrated* (*UMI*) *Simulation*, consists of the following processes. At each time step of numerical simulation, the difference between the measurable output signal and the signal indicated by numerical simulation is evaluated. Feedback signals are generated from the difference, and numerical simulation is updated applying the feedback signal to compensate for the difference. This paper deals with a numerical study on the fundamental characteristics of UMI simulation using a simple two-dimensional model problem for the blood flow in an aorta with an aneurysm. The effect of the number of feedback points and the feedback formula are investigated systematically. It is revealed that the result of UMI simulation in the feedback domain rapidly converges to the standard solution, even with usually inevitable incorrect upstream boundary conditions. Finally, an example of UMI simulation with feedback from real color Doppler measurement also shows a good agreement with measurement.

Keywords—Bio-fluid mechanics, Computational fluid dynamics, Ultrasonic measurement, Color Doppler imaging, Measurement-integrated simulation, Aneurysm, Boundary condition, Pulsatile flow.

INTRODUCTION

Blood flow, which plays important roles in vital sustentation and homeostasis, is hindered by disabilities resulting from circulatory diseases.[22] For example, with aging, asymptomatic aneurysms may develop due to arteriosclerosis, and their rupture may be fatal. It has been empirically found that the size of aneurysms is a reliable anatomical factor predictive of rupture, and statistics have been compiled regarding the size of ruptured and unruptured aneurysms.[27,29] For example, Ujiie *et al*. suggested that the aspect ratio of aneurysms is a useful parameter in predicting imminent aneurysmal rupture.[29] Although hemodynamic forces such as blood pressure and wall shear stress due to blood flow are known to be related to the development, progress, and rupture of aneurysms,[2,7,14,25] detailed mechanisms remain to be elucidated. Clarification of the relationship between pathology and the cause of circulatory diseases is essential.

Among a number of existing imaging modalities, color Doppler ultrasonography is widely used for the diagnosis of blood vessel diseases since it noninvasively provides real-time images of the blood flow structure and vessel configuration by a relatively compact system. Figure 1 shows an example of a color Doppler image around an aneurysm of the descending aorta. The configuration of the vessel wall is reconstructed as a B-mode image from time delays and magnitudes of the ultrasonic echo, which are emitted from a probe (located at the center of the sector), and reflected by the structures *in vivo*. Furthermore, the blood velocity component in the direction of the ultrasonic beam or the Doppler velocity is measured by the Doppler shift frequency. In order to visualize the blood flow, the frequency shifts are converted to colors of graduated intensity, blue for flow away from the probe and red for flow approaching the probe, as displayed on top of the B-mode image. Since the equipment measures only the Doppler velocity, it is difficult to recognize the exact three-dimensional blood flow field. Recently, three-dimensional reconstruction of the blood vessel configuration, velocity profile, and pressure distribution from the ultrasonic measurement have been investigated.[1,18,21,28] Capineri *et al*. developed a technique for dynamic displays of vector velocity maps, in which the velocity vectors obtained by Doppler measurements in two independent directions are properly interpolated.[1] Tortoli *et al*. presented the real-time two-dimensional velocity profile of descending aortic blood flow using a set-up based on an esophageal probe connected to a multigate Doppler-processing system, and confirmed extremely complex flow in the proximal

Address correspondence to Dr. T. Hayase, Institute of Fluid Science, Tohoku University, 2-1-1 Katahira, Aoba-ku, Sendai 980-8577, Japan. Electronic mail: hayase@ifs.tohoku.ac.jp

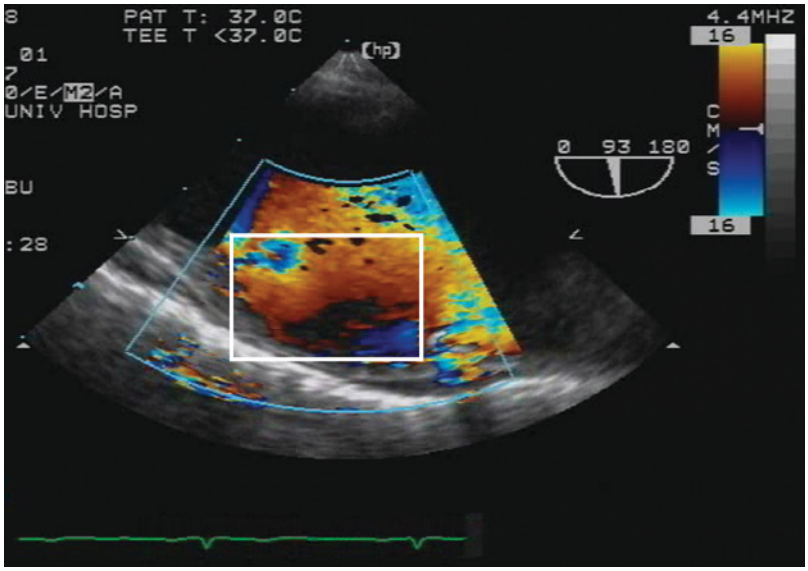

FIGURE 1. Color Doppler image around a thoracic aneurysm (Center frequency: 4.4 MHz, Pulse repetition frequency: 4 kHz).

portion of the aortic arch or in the case of aortic diseases.[28] Ohtsuki *et al*. developed a new method for nondisturbing, quantitative measurement of pressure, in which the velocity component orthogonal to the Doppler velocity is deduced after measurement of the velocity field by the pulse Doppler technique, and the pressure is calculated from the acceleration.[18] However, in experimental works, there are some limitations such as the direct effects of noise and the Doppler transducer position on data acquisition and the assumption of symmetrical flow in the calculation, so that no method to obtain complete information in real time yet exists.

As a counterpart of measurement, numerical simulation of the blood flow has been studied extensively. Realistic representation of blood flow can be obtained by solving the fundamental equations of the flow with realistic vessel geometries obtained by medical imaging techniques such as magnetic resonance imaging (MRI) or computed tomography (CT).[3,4,8,12,15,16,24,26,30] Numerical simulation dealing with flow in an aorta with an aneurysm has also been carried out by such a combination.[3,4,26] Taylor and Yamaguchi reported the appearance and disappearance of a primary vortex and regions of high shear stresses both at the proximal and distal ends of the aneurysm.[26] Di Martino *et al*. studied the complex mechanical interaction between blood flow and wall dynamics in a three-dimensional custom model of an abdominal aortic aneurysm and provided a quantitative local evaluation of the stresses.[3] However, numerical simulation has an inherent problem of specification of the boundary conditions,[8,12,15,16] and thus the calculated blood flow is usually similar but not identical to the real one. In order to minimize the effect of inaccurate inlet velocity profile specification on local wall shear stress computations in the vessel segment, Liu *et al*. extended their model of the carotid artery in the upstream direction with a straight tube, proposing that such extension may be useful until more accurate, noninvasively obtained velocity profile data for the inlet become available.[15] In the descending aorta, however, extension by adding the ascending aorta and the aortic arch does not eliminate the effect of the upstream boundary condition on reproduction of the complicated flow structure (e.g., Kilner *et al*. observed helical and retrograde secondary flow patterns in the aortic arch using magnetic resonance velocity mapping).[13,28] By numerical simulation with an integrated model of the left ventricle and the aorta, Nakamura *et al*. revealed that the upstream boundary condition strongly influences development of the helical flow.[16] Glor *et al*. performed MRI velocity measurements and computation in the U bend, confirming the importance of accurate inflow boundary conditions.[8] Since velocity data cannot yet be reliably measured by MRI due to artifacts such as partial volume effect, inevitable errors are introduced to the computation of the full three-dimensional velocity field and wall shear stress. Therefore, development of new methodology that can exactly provide detailed information on blood flow is strongly required.

Integration of computation and measurement in the framework of a flow observer is a possible way to solve these problems.[9,17] Hayase *et al*. proposed such a flow observer as an analytic methodology for general flow problems.[9] Conceptually, a flow observer is the state observer in control theory applied to flow analysis. For investigation of a real flow, a simulation model is constructed in a computer using standard numerical analysis methodology based on fundamental equations with appropriate boundary and initial conditions. Some output signals are defined for real flow measurement and for numerical simulation

in order to evaluate the difference between the two results. Numerical simulation is carried out with an additional body force or a boundary condition as a feedback signal that is derived from the difference between the two output signals. If the feedback law is designed properly, the computational result converges to the real flow. In the cited study by Hayase *et al*.,[9] numerical simulation of the flow observer was performed for a turbulent flow through a square duct. Turbulent flow structure including fluctuation was successfully reproduced by the feedback of errors in the axial velocity components estimated at 100 points on a cross section of the duct to the pressure boundary condition based on the simple proportional control law. Nisugi *et al*. developed a hybrid wind tunnel based on a flow observer and investigated the flow with a Karman vortex street, revealing the substantial advantage of such methodology over ordinary simulation, especially in its ability to reconstruct real flow and in its computational efficiency.[17] As a flow analysis method, a flow observer generally has several advantages: (1) simulation is performed using real flow conditions, (2) the simulation is simultaneously validated by measurement, and (3) real-time simulation can possibly be carried out owing to a significant improvement in computational efficiency.

In this paper, a flow observer is applied for the analysis of blood flow by integrating numerical simulation and measurement with color Doppler ultrasonography. We term this method Ultrasonic-Measurement-Integrated (UMI) simulation. In UMI simulation, feedback signals are added to the Navier-Stokes equation and the pressure equation in the form of a source term to compensate for the difference between the computation and the measurement. Of course, UMI simulation is expected not only to reconstruct the color Doppler image but also to provide the velocity vectors and the pressure distribution in detail. This paper concerns UMI simulation using a simple two-dimensional model problem for blood flow in an aorta with an aneurysm. We focus on the problem of whether the feedback loop in UMI simulation effectively reduces the error in the flow domain resulting from an incorrect velocity profile setting at the upstream boundary, which usually takes place in numerical simulations of blood flow. A numerical simulation with an assumed boundary condition is first defined as a model of real flow since existing ultrasonic measurement does not provide complete information on real blood flow and, therefore, is not suitable as a standard to evaluate UMI simulation. UMI simulation is investigated as to the convergence of its result to the standard solution when the real velocity profile at the upstream boundary is unknown and is incorrectly assumed. Feedback algorithms of UMI simulation are designed by evaluating the error from the standard solution. Using these feedback algorithms, an example of UMI simulation with the feedback using real color Doppler measurement is also presented.

UMI SIMULATION USING SIMULATED COLOR DOPPLER MEASUREMENT

Subject and Computational Method

This paper deals with the blood flow in the vicinity of an aneurysm in the descending aorta as shown in Fig. 1. A 62-year-old male patient with a chronic aortic aneurysm in his descending aorta participated in the study. He had no significant cardiac complications. His cardiac output was 9.17×10^{-5} m^3 s^{-1} (5.5 l min^{-1}) and his heart rate was 0.87 Hz (52 bpm) during the measurement. Transesophageal echocardiography was performed with an ultrasound device (SONOS 5500, Philips Medical Systems, Andover, MA, USA) with a transesophageal ultrasonic transducer (T6210, Philips Medical Systems, Andover, MA, USA). The central frequency was variable, ranging from 4 to 7 MHz. The images were stored with a digital video recorder (DCR-TRV30, SONY, Tokyo, Japan). In UMI simulation, the B-mode image of the blood vessel obtained by ultrasonic diagnostic equipment is digitized to extract the cross-sectional surface manually, and the pixel data is allocated to define a two-dimensional computational domain. The shape of the blood vessel is extended in both the upstream and downstream directions in order to perform numerical simulation (see Fig. 2, the right side is upstream). The x-axis is defined in the flow direction at the upstream boundary ($x = 0$), and the y-axis is defined against it with the left-handed system.

Table 1 shows parameters used in this computation. Cardiac cycle T is calculated from the heart rate. The upstream shape of the blood vessel is assumed to be cylindrical, and the diameter D is calculated from the image. Since the upstream boundary is located at some distance from the aneurysm, we consider that the blood vessel can be assumed to be cylindrical. Three-dimensional reconstruction from B-mode images in many directions may give the correct shape of the cross section. We are not, however, so concerned with this since this paper deals with

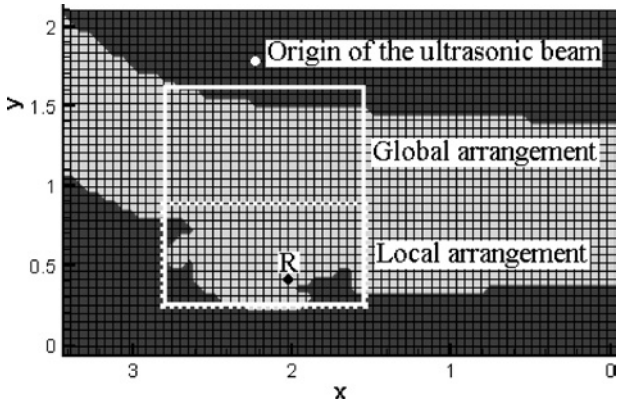

FIGURE 2. Computational grid and arrangement of monitoring points.

TABLE 1. Computational conditions.

Heart rate	0.87 Hz (52 bpm)
Cardiac cycle T	1.15 s
Cardiac output	9.17×10^{-5} m^3/s (5.5 l/min)
Entrance flow	6.42×10^{-5} m^3/s (3.85 l/min)
Maximum mean velocity $u'_{\max}$	0.74 m/s
Entrance vessel diameter D	28.25×10^{-3} m
Kinematic viscosity ν	4.0×10^{-6} m^2/s

fundamental two-dimensional analysis. With reference to the blood flow measurement data, we assume that 30% of the cardiac output flows into the branches and that the remaining 70% (6.42×10^{-5} m^3 s^{-1}) flows into the descending aorta.[6] The variation of the flow rate q is modeled as shown in Fig. 3 according to the MR measurement by Olufsen *et al.*[19] Blood is assumed to be Newtonian fluid with a density $\rho = 1.00 \times 10^3$ kg m^{-3} and a dynamic viscosity $\mu = 4.0 \times 10^{-3}$ Pa s within normal range.

As a fundamental consideration of blood flow simulation integrated with ultrasonic measurement, we assume two-dimensional flow, although intravascular blood flow *in vivo* has a complex three-dimensional structure. Governing equations for two-dimensional incompressible and viscous fluid flow are the Navier-Stokes equation,

$$\frac{\partial \mathbf{u}}{\partial t} = -(\mathbf{u} \cdot \mathrm{grad})\,\mathbf{u} + \frac{1}{Re}\nabla^2 \mathbf{u} - \mathrm{grad}\, p, \qquad (1)$$

and the equation of continuity,

$$\mathrm{div}\,\mathbf{u} = 0, \qquad (2)$$

where $\mathbf{u} = (u, v)$ is the velocity vector and p is the pressure. All the values are nondimensionalized with the diameter of the blood vessel D, the cross-sectional average velocity $u_{\max}$ at the upstream boundary for the maximum cardiac output, and the kinematic viscosity ν of the blood. From here on, the same symbols are used for both dimensional and nondimensional values since it does not cause confusion.

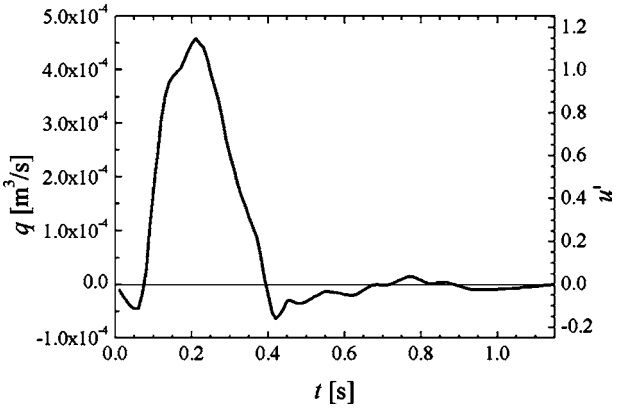

FIGURE 3. Time variation of flow volume in descending aorta and of cross-sectional average flow velocity at upstream boundary (nondimensional).

With regard to the upstream boundary conditions for the standard solution, we assume a Poiseuille flow with a parabolic profile in x-directional velocity. For the condition of UMI simulation and the ordinary simulation, in contrast, we assume a different flow with a uniform profile in x-directional velocity.

$$u(X_\mathrm{u}, y, t) = \begin{cases} \frac{3}{2}u'(t)\{1 - (y - Y_\mathrm{u})^2/(D/2)^2\} & \text{(Standard solution)} \\ u'(t) & \text{(UMI simulation and ordinary simulation)} \end{cases}$$
$$v(X_\mathrm{u}, y, t) = 0\,, \qquad (3)$$
$$Y_\mathrm{u} - D/2 \le y \le Y_\mathrm{u} + D/2$$

where X_u and Y_u are the x and y coordinates of the center of the vessel at the upstream boundary, respectively, and $u'(t)$ is the time-varying upstream cross-sectional average flow velocity determined by the modeled flow rate[19] as shown in Fig. 3. As mentioned above, we define the standard numerical solution as a model of the real flow. In order to investigate the effect of the feedback signal on UMI simulation, its upstream boundary velocity profile is assumed to be different from that of the standard solution. At the downstream boundary of the computational domain, the free-flow condition ($\partial/\partial n = 0$, n: coordinate normal to the boundary) is applied, and the no-slip condition is applied to the blood vessel wall.

The governing equations are discretized by means of the finite volume method. These equations are solved with an algorithm similar to the SIMPLER method.[10,20] In the SIMPLER method, the x-directional momentum equation in Navier-Stokes equations is expressed as

$$u_i = \left(\sum B_j u_j + S_i\right) \Big/ B_i + d_i(p_i - p_{i-1}), \qquad (4)$$

where $\left(\sum B_j u_j\right)$ means the summation of the values at four adjacent nodes. By substituting Eq. (4) and similar equations for y-directional momentum to the integrated form of the equation of continuity, the pressure equation is obtained.

$$a_i p_i = \sum a_j p_j + s_{pi}\,, \qquad (5)$$

where $\left(\sum a_j p_j\right)$ represents the summation of the values at four adjacent nodes. The concrete notations of the parameters in Eqs. (4) and (5), as well as supplementary pressure correction equations and velocity correction procedure in the SIMPLER method, are explained in a reference.[20] In descretization of the convective terms in Navier-Stokes equations, a consistently reformulated QUICK scheme[11] is applied in order to assure continuity of the flux at the interface of control volumes during the iterations. The QUICK scheme is a three-point upstream-weighted quadratic interpolation technique within the context of a control-volume approach. In the discretization for the time derivative terms, a second order implicit scheme[5] is used. The system of linear algebraic equations is solved with the pentadiagonal matrix solver, i.e., the MSI method,[23] which is a very efficient iterative solver of linear equations.

In this study, we introduced three types of staggered grid systems, in which nodes for velocity components are shifted in half grid size from the pressure node, with different numbers of grid points in the x and y directions: 32×20 with grid spacing of 2.973×10^{-3} m (Grid A), 65×40 with 1.487×10^{-3} m (Grid B), and 130×80 with 0.743×10^{-3} m (Grid C). Among these three types of grid systems, Grid A is too coarse to represent the shape of the blood vessel precisely. On the other hand, Grid C is fine enough to represent the shape, but it requires huge computational time (about 300 h for one case) to converge to the periodic solution. Hence, in the numerical study for the validation of UMI simulation, we use Grid B as shown in Fig. 2, compromising between reproducibility of the vessel shape and computational time. The adequate residual at convergence and the maximum iteration number are respectively determined as 1×10^{-5} and 300 after test computations.

Feedback Law

In designing UMI simulation, we define monitoring points in the relevant flow domain. At the monitoring points, output signals are evaluated both in ultrasonic measurement and simulation. Feedback signals, derived from the difference between these output signals, are applied to the computation in order to compensate for the computational error and to make the computational result converge to the real flows. In the present study, the real flow is modeled as the standard numerical solution, and the error of UMI simulation is due to an inaccurate boundary condition as mentioned above. For the validation of UMI simulation, we define two arrangements of monitoring points: 1) global arrangement, all 675 grid points in the large rectangle region which covers the blood vessel near the aneurysm in Fig. 2, and 2) local arrangement, all 325 points in the small rectangle above the aneurysm in Fig. 2.

Figure 4 explains how we calculate the feedback signal. The velocity vector obtained by the numerical simulation

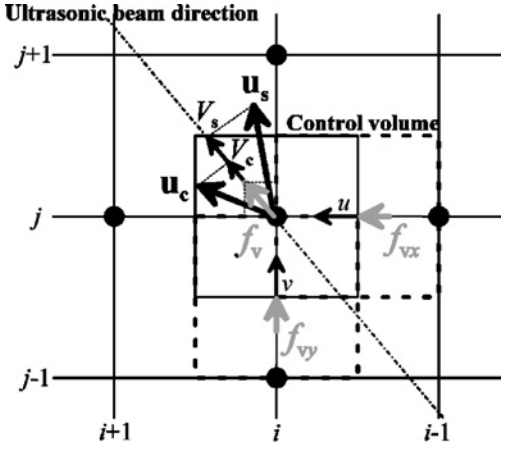

FIGURE 4. Schematic diagram of calculation of feedback signals.

is defined as $\mathbf{u}_c$, and that of the standard solution (model of the real flow) is $\mathbf{u}_s$. The purpose of the feedback is to force the velocity $\mathbf{u}_c$ to converge to $\mathbf{u}_s$. Doppler velocity of the blood flow is obtained with ultrasonic diagnostic equipment. The Doppler velocities of the numerical simulation and the standard solution, V_c and V_s, are the projection of $\mathbf{u}_c$ and $\mathbf{u}_s$ in the ultrasonic beam direction (a chain line in Fig. 4), respectively. Here, it should be noted that Doppler velocities V_c and V_s each represent only one component of the velocity vector, and, therefore, it is not a straightforward task to reconstruct the velocity vectors from the Doppler velocities. In other words, the velocity vector $\mathbf{u}_s$ is generally unknown in real ultrasonic measurement. In the staggered grid system used in the SIMPLER method, node points for velocity components u and v are shifted from the pressure node, "•", in half mesh size. Therefore, the velocity components at the pressure node are evaluated by interpolation in the above description. The origin of the ultrasonic beam, where ultrasound is emitted from the probe, is set at the same position as that of the measurement (the center of the sector in Fig. 1).

In this study, we deal with two feedback algorithms, feedback to velocity field (feedback A) and feedback to velocity and pressure fields (feedback B), as follows.

Feedback A: *As the feedback signal, the artificial force f_v proportional to the difference between Doppler velocities of the standard solution and UMI simulation is applied to the Navier-Stokes equation in the direction of the ultrasonic beam.*

In this formula, the force f_v is calculated by the following equation:

$$f_v = -K_v \rho (V_c - V_s) u'_{max} \Delta S, \tag{6}$$

where K_v is the feedback gain (nondimensional), u'_{max} is the maximum average flow velocity of the blood at the upstream boundary, and ΔS is an interfacial area of the control volume of pressure. Referring to Fig. 4, if the computational result V_c is smaller than V_s, the artificial force f_v has a positive value and accelerates the fluid along the ultrasonic beam in UMI simulation to reduce the error. The force f_v is decomposed to the x-directional component f_{vx} and the y-directional component f_{vy}, which are added to the control volumes of $u(i, j)$ and $v(i, j)$ in the Navier-Stokes equation, respectively.

Feedback B: *In feedback A, artificial forces f_{vx} and f_{vy} not only accelerate the fluid to reduce the error in velocity but also increase the pressure of the control volume (i, j) through the pressure equation derived from the equation of continuity in the SIMPLER method.*[20] *Hence, we introduce additional feedback to the pressure equation to counteract the effect of artificial force f_v.*

In this formula, a source term s_p, proportional to the difference between the Doppler velocities, is added to the pressure equation and calculated artificial force f_v is added to the Navier-Stokes equation in feedback A:

$$\begin{aligned} f_v &= -K_v \rho (V_c - V_s) u'_{max} \Delta S \\ s_p &= -K_p \rho (V_c - V_s) \Delta S \end{aligned}, \tag{7}$$

where K_p is the feedback gain for the pressure (nondimensional).

UMI simulation with feedback B is specified by the combination of gains (K_v, K_p). Note that the special case with $K_p = 0$ corresponds to feedback A, and $K_v = K_p = 0$ corresponds to the ordinary simulation without feedback.

Evaluation Method

In order to evaluate the accuracy of UMI simulation, we define the error norm e_n for an arbitrary variable a, which is the velocity component u, v, V, or the pressure p, by the following equation:

$$e_n = \frac{1}{a_{max} T} \int_T |a_{cn}(t) - a_{sn}(t)| \, dt, \tag{8}$$

where T is the cardiac cycle, a_{max} is the characteristic value for normalization: $a_{max} = u'_{max}$ for velocity or $a_{max} = \rho {u'_{max}}^2$ for pressure, where u'_{max} is the maximum average flow velocity at the upstream boundary. Subscript cn corresponds to UMI simulation or ordinary simulation, and sn corresponds to the standard solution, respectively. In the subscripts "cn" and "sn," n is the index of the grid point.

The average error norm $\bar{e}_N$ is evaluated over the monitoring points in a domain.

$$\bar{e}_N = \frac{1}{N} \sum_n e_n. \tag{9}$$

In this section, 675 monitoring points in the global arrangement or 325 points in the local arrangement are used for the calculation of $\bar{e}_N$, and they are called $\bar{e}_{675}$ or $\bar{e}_{325}$, respectively.

The optimum values of the gain K_v for feedback A and the combination of gains (K_v, K_p) for feedback B are determined so that the average error norms $\bar{e}_N$ of some specified variables take the minimum value over a number of trial computations.

The accuracy of UMI simulation is evaluated by comparing the average error norms $\bar{e}_N$ of UMI simulation for velocity components, Doppler velocity, and pressure, against those of the ordinary simulation without feedback.

Results and Discussion

The standard solution is first obtained from the numerical simulation with the upstream parabolic velocity profile. Solid lines in Fig. 5 represent the velocity components and

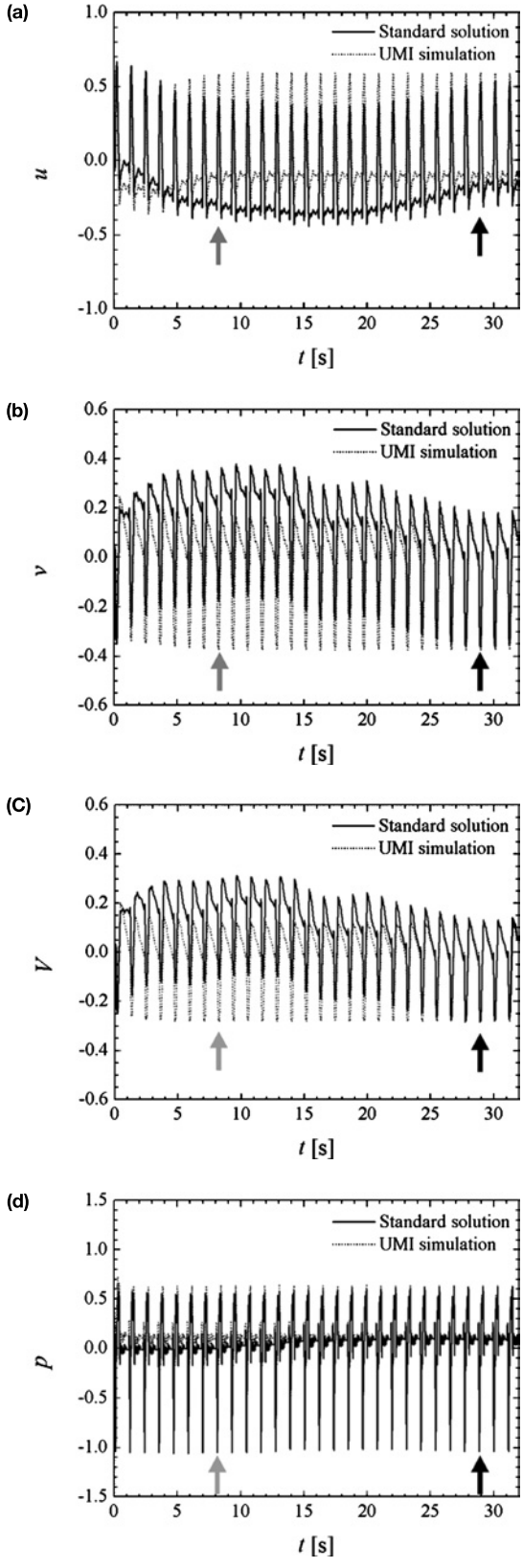

FIGURE 5. Comparison of convergence with periodic solutions regarding (a) *x*-directional velocity *u*, (b) *y*-directional velocity *v*, (c) Doppler velocity *V*, and (d) pressure *p* (all results are nondimensional).

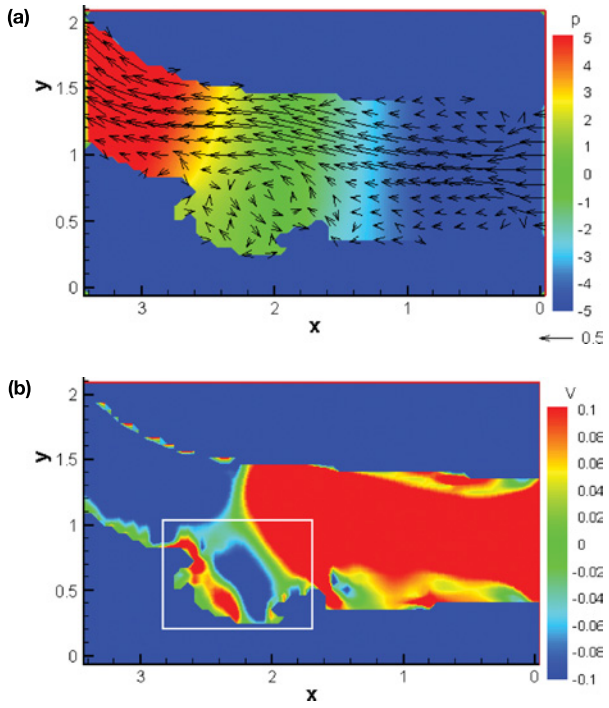

FIGURE 6. (a) Velocity vectors and pressure distribution and (b) color Doppler image of the standard solution at $t = 0.35$s in deceleration phase (all results are nondimensional).

the pressure for 32 s (about 28 cardiac cycles) at one monitoring point R (see Fig. 2). The results of UMI simulation shown by dotted lines are discussed later in this section. In 26 cardiac cycles, the solution converges to almost periodic oscillation (black arrows). We define the standard solution as the repetition of the result in the 26th cardiac cycle. Figure 6 shows velocity vectors, pressure distribution, and the color Doppler image of the standard solution at $t = 0.35$ s in the deceleration phase (see Fig. 3). It is noted that the color Doppler image representing only one velocity component does not show the structure of the blood velocity vector field. For example, vortices above the aneurysm are displayed by a mosaic pattern consisting of red and blue regions (as can be seen in the white rectangle in Fig. 6).

UMI simulation was performed with the above-mentioned standard solution and the feedback algorithm A in Eq. (6), as well as with the feedback algorithm B in Eq. (7). For a given value of K_v in feedback A or (K_v, K_p) in feedback B, time-dependent calculation was carried out until periodical oscillations were obtained, and the average error norm $\bar{e}_N$ was evaluated using a periodical solution. Figure 7 shows the average error norm $\bar{e}_{675}$ with the global arrangement of the monitoring points (see Fig. 2) for the Doppler velocity, x and y-directional velocity components, and the pressure as a function of the gain K_v. Note that we investigated only the limited case of $K_v = K_p$ for feedback B. Study of the full (K_v, K_p) parameter plane remains as a future work.

In the figures on the left-hand side of Fig. 7 (a), the average error norm $\bar{e}_{675}$ of the Doppler velocity for feedback A monotonically decreases as the feedback gain increases in the range of $0 \le K_v \le 7$. Over $K_v = 8$, UMI simulation begins to diverge, and $\bar{e}_{675}$ shows a steep increase. The figures on the right-hand side are magnifications of the region $0 \le K_v \le 1$ in order to show the result of feedback B clearly. The result for feedback B shows a faster reduction, but it undergoes sudden divergence at some critical value of K_v. The average error norms $\bar{e}_{675}$ of the velocity components u and v show changes similar to that of the Doppler velocity [Fig. 7(b)]. The error of the pressure, however, takes the minimum value at a relatively small K_v value [Fig. 7(c)]. Considering these results, the optimum gains for feedback A and B are determined with the average error norms $\bar{e}_N$ for the l_1 norm ($|u| + |v|$) of the velocity vector. The optimum feedback gain K_v with the global arrangement is determined as $K_v = 7$ for feedback A, and $K_v = K_p = 0.3$ for feedback B. Note that the optimum gains change if the average error norm of the pressure is taken into account, especially for feedback A.

In order to evaluate the validity of the present UMI simulation, the error of UMI simulation against the standard solution is compared with that of the ordinary numerical simulation. The color Doppler images around an aneurysm at $t = 0.35$ s in the deceleration phase of the cardiac cycle are compared in Fig. 8. The mosaic pattern of the aneurysm, which implies a disturbed flow structure such as vortices (see Fig. 6), is different between the ordinary simulation [Fig. 8(b)] and the standard solution [Fig. 8(a)] since the upstream boundary condition is different. On the other hand, the color Doppler images of UMI simulations with both feedback A [Fig. 8(c)] and B [Fig. 8(d)] closely resemble that of the standard solution in the aneurysm despite the upstream boundary condition being different. The same mosaic pattern in the aneurysm implies correct reproduction of the blood flow structure.

Variations of the velocity components and the pressure at the monitoring point R (see Fig. 2) in a cardiac cycle are compared between the standard solution, UMI simulations of feedback A and B, and the ordinary simulation in Fig. 9. Due to the incorrect upstream boundary condition, the result of the ordinary simulation is different from that of the standard solution. In contrast, in spite of the same incorrect boundary condition, excellent agreement is attained by UMI simulation with feedback A with regard to the velocity components u and v, as well as Doppler velocity. UMI simulation with feedback B also shows results very close to those of the standard solution except for u. In the velocity components of UMI simulation with feedback B, Doppler velocity V agrees with that of the standard solution the best since this study, uses it as the output signal for the feedback artificial force is applied in the ultrasonic beam direction in UMI simulation. The y-directional velocity component v shows better agreement with the standard solution than does

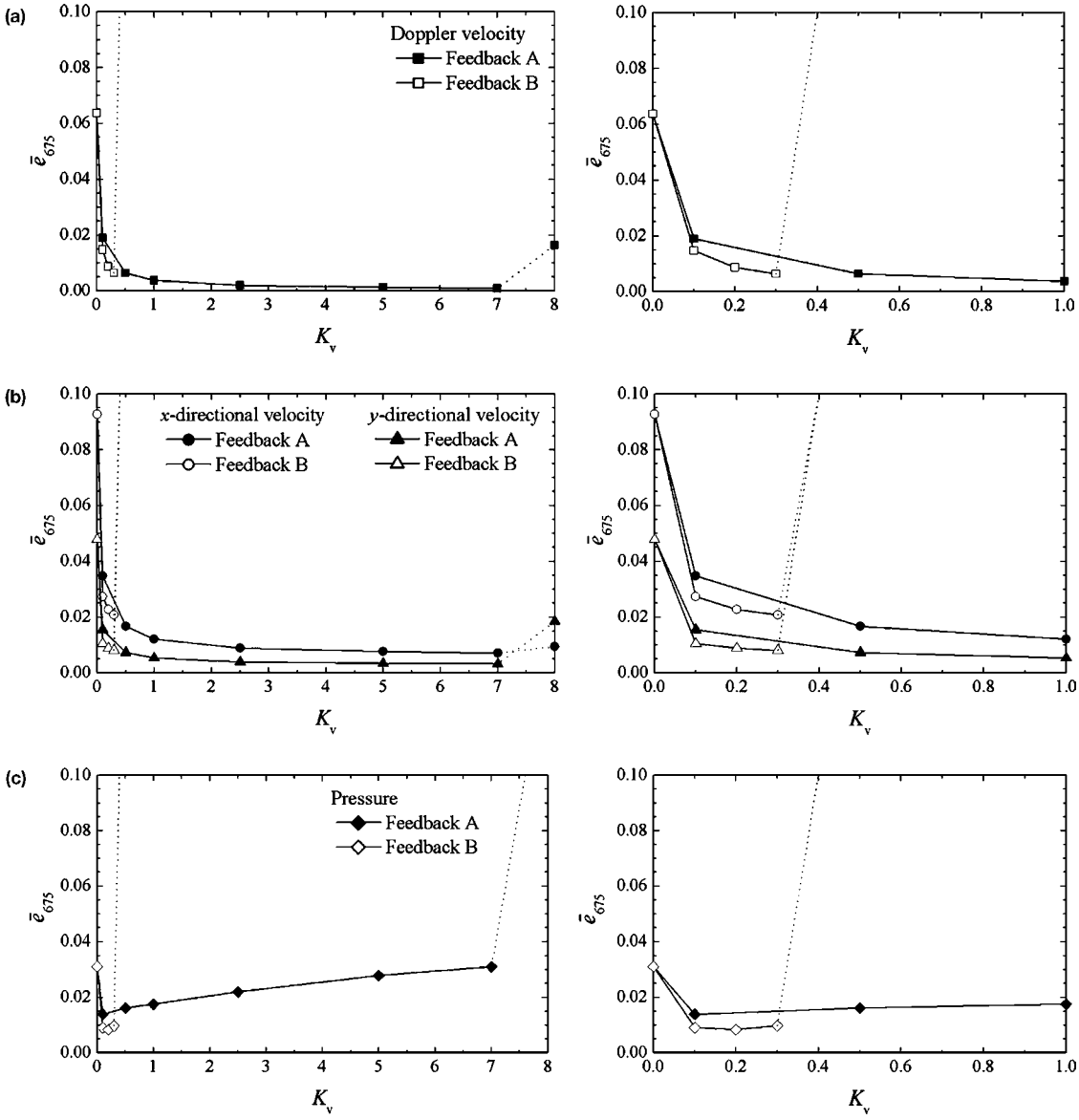

FIGURE 7. Variation of average error norm $\bar{e}_{675}$ of (a) Doppler velocity, (b) *x*, *y*-directional velocity components, and (c) pressure against feedback gain K_V in UMI simulation with global arrangement of monitoring points. Figures on right-hand side show $0 \leq K_V \leq 1.0$ magnification.

the *x*-directional velocity component *u*. This is because the origin of the ultrasonic beam is away from the monitoring points in the *y*-direction and, therefore, the Doppler velocity at each monitoring point mainly consists of the *y*-directional velocity component. This means that the computational accuracy of the *x*-directional velocity component could possibly be improved if the origin of the ultrasonic beam were moved to change the angle of the ultrasonic beam so that the Doppler velocity would contain more of the *x*-directional velocity component. The variation of the pressure clearly shows the difference between the two feedback formulae. The result of feedback formula A shows poorer agreement than the ordinary simulation, while that of feedback formula B shows fairly good agreement with that of the standard solution. Generally, feedback A can reproduce the velocity components excellently while feedback B can reproduce both the velocity components and the pressure.

Figure 10 compares the distribution of the error norm in the blood vessel around the aneurysm for the velocity components and pressure between the ordinary simulation and UMI simulation with two monitoring point arrangements and two feedback formulae. In the result of the ordinary simulation, the area of large error shown in red appears in the aneurysm for all velocity components and in the upper side of the blood vessel for *x*-directional velocity component *u*. For the pressure, an area with relatively

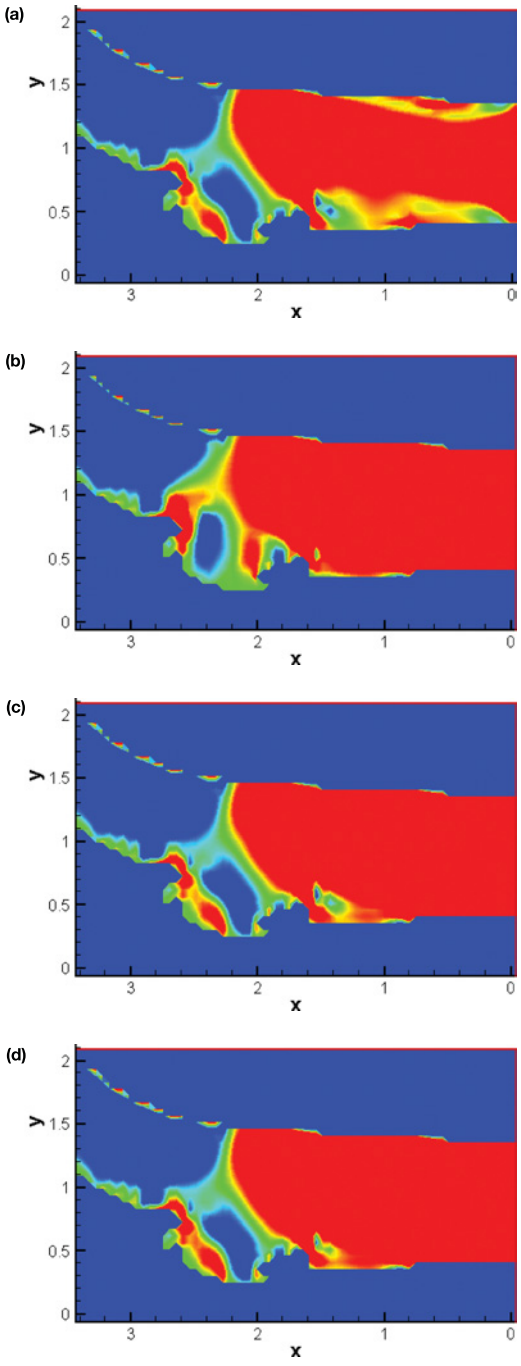

FIGURE 8. Comparison of color Doppler images at $t = 0.35$s in deceleration phase among (a) standard solution, (b) ordinary simulation, and (c) and (d) UMI simulations with feedback A and B, respectively. Feedback A: $K_v = 7$, feedback B: $(K_v, K_p) = (0.3, 0.3)$. Color bar is the same as that in Fig. 6 (b).

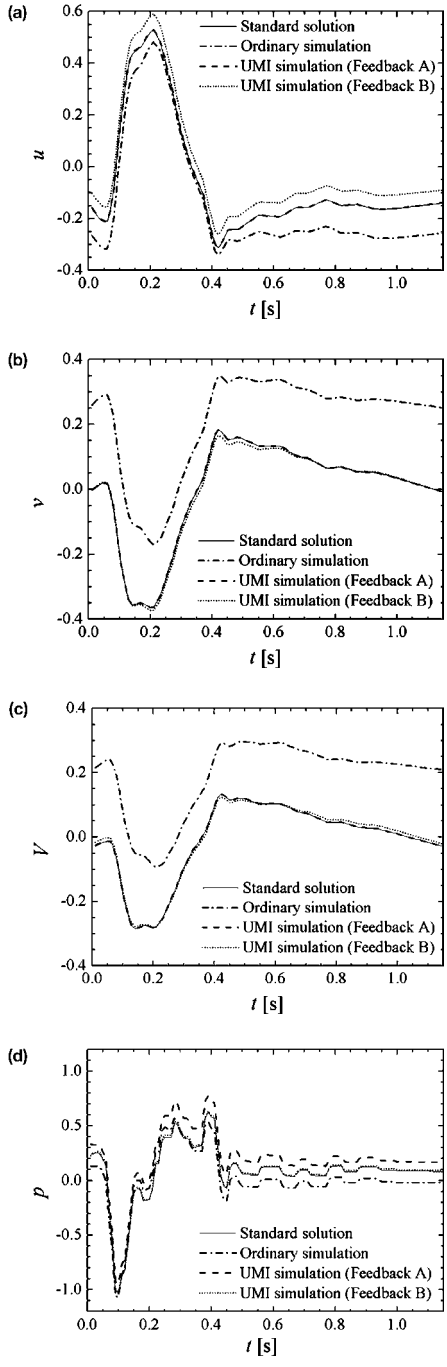

FIGURE 9. Comparison of periodic solutions of (a) *x*-directional velocity *u*, (b) *y*-directional velocity *v*, (c) Doppler velocity *V*, and (d) pressure *p* at monitoring point R (all results are nondimensional). Feedback A: $K_v = 7$, feedback B: $(K_v, K_p) = (0.3, 0.3)$.

large error exists in the downstream region of the computational domain. In the result of feedback A with global arrangement, a fairly good result is obtained for all the velocity components. The error norm, indicated by blue, is reduced to almost zero. In the result for the pressure, however, the error is larger than that of the ordinary simulation in the aneurysm. A better result for the pressure is obtained with feedback formula B with global arrangement. The errors of the *y*-directional velocity component v and the Doppler velocity V are almost the same as those in the former case, although the error of the *x*-directional velocity component u is somewhat larger than that in the former case but still smaller than that of the ordinary simulation.

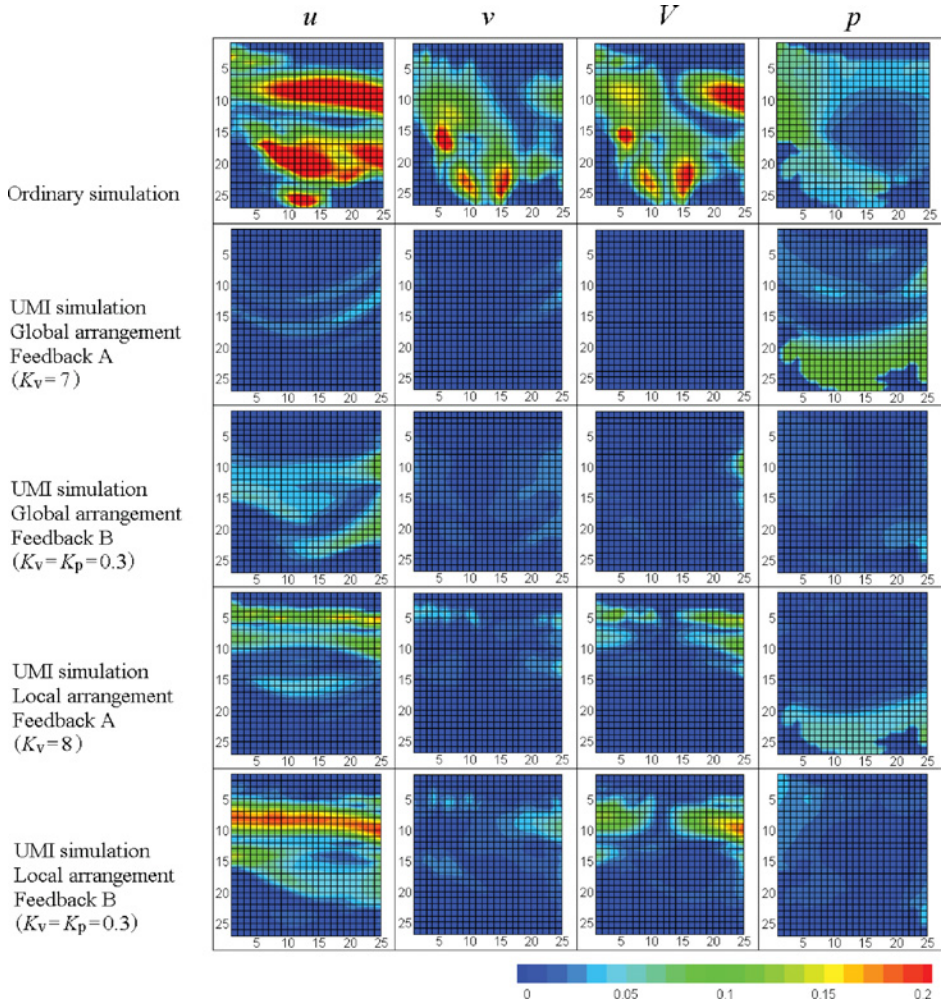

FIGURE 10. Comparison of error norms between the ordinary simulation and UMI simulations with feedback A and B using global and local arrangements.

The results of UMI simulation with the local arrangement of the monitoring points are also given in Fig. 10. For obtaining the optimum gain for the case of local arrangement, systematic computation was performed in a way similar to that in Fig. 7. With the local arrangement of the monitoring points (Fig. 2), the optimum gains, which minimalize the average error norms $\bar{e}_{325}$ for the l_1 norm ($|u| + |v|$) of the velocity vector, is $K_v = 8$ for feedback A and $K_v = K_p = 0.3$ for feedback B. In all results, reduction of the error norm e_n is significant in the aneurysm where the monitoring points are arranged. As has been mentioned, feedback A gives a better result for x-directional velocity u, while feedback B is better for the pressure p.

Table 2 summarizes the average error norms of velocity components and pressure normalized with the results of the ordinary simulation. Note that the smallest error in each comparison is shaded. The smallest errors of $\bar{e}_{675}$ for the velocity components are obtained by feedback A using the global arrangement of the monitoring points. In this case, UMI simulation reduces the error $\bar{e}_{675}$ to 8% for u, 7% for v, and 2% for V of those of the ordinary simulation. Comparison between the results with feedback formulae A and B reveals that feedback A is superior to feedback B for reproduction of the velocity components, but is inferior for the reproduction of the pressure. UMI simulation with feedback B using the global arrangement of monitoring points reduces the error $\bar{e}_{675}$ to 32% for p of that of the ordinary simulation. As for the arrangement of the monitoring points, the local arrangement, which seems more realistic in practical application of UMI simulation using color Doppler measurement, yields a poorer result than the global arrangement for the global error $\bar{e}_{675}$, but gives comparatively good results if evaluated by the localized error $\bar{e}_{325}$. This implies that we may locally arrange the monitoring points in the region of concern.

Finally, the computational load of UMI simulation is discussed in comparison with ordinary simulation. In Fig. 5, the dotted lines represent the velocity components and the pressure of the result of UMI simulation with feedback B of the gain $(K_v, K_p) = (0.3, 0.3)$ using the global arrangement

TABLE 2. Comparison of average error norm.

Monitoring point arrangement	Feedback	u	v	V	p
$\bar{e}_{675}$					
None	None[a]	1	1	1	1
Global	A	0.078	0.069	0.015	0.997
	B	0.224	0170	0.102	0.315
Local	A	0.279	0.152	0.217	0.482
	B	0.503	0.216	0.354	0.330
$\bar{e}_{325}$					
None	None[a]	1	1	1	1
Global	A	0.066	0.036	0.016	1.701
	B	0.223	0.137	0.107	0.358
Local	A	0.093	0.047	0.012	0.935
	B	0.229	0.113	0.085	0.312

[a]Ordinary simulation.

of the monitoring points. The periodic solution is obtained in eight cycles (see gray arrows in Fig. 5), implying that UMI simulation requires less than one-third the computational time steps than the ordinary simulation for 26 cycles to obtain steady oscillation. As for computational time, however, the standard solution requires 4500 s for one cardiac cycle T in comparison with UMI simulation, which requires 6300 s. The time required by UMI simulation is 1.4 times longer than that for the ordinary simulation for 1 cardiac cycle. Consequently, UMI simulation shortens the computational time to obtain the periodic solution by a factor of 0.4. It is noted that computational load of UMI simulation depends on the feedback formula and the number of monitoring points. UMI simulation with feedback B requires more computational time than that with feedback formula A. For example, UMI simulation using feedback formula A with the global arrangement of monitoring points takes 5000 s for one cardiac cycle, which is slightly longer than the time required by the ordinary simulation.

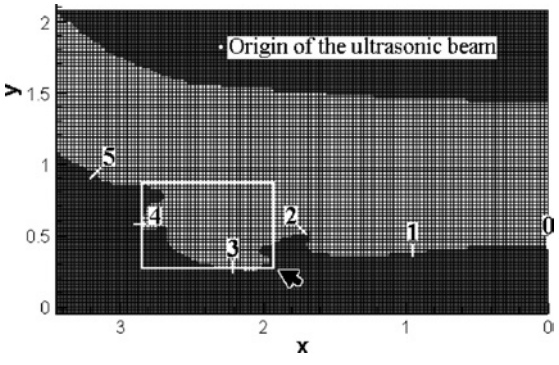

FIGURE 11. Computational grid used for UMI simulation using real color Doppler measurement. The marked numbers are the length along the blood vessel wall measured from the upstream boundary.

UMI SIMULATION USING REAL COLOR DOPPLER MEASUREMENT

Computational Method

In this section, we perform UMI simulation using real color Doppler measurement. The medical data of the patient, instrument, and equipment are all identical to those of the previous section. As a fundamental consideration, the analysis is limited to a two-dimensional flow problem. The result of UMI simulation is compared with those of the ordinary simulation and the real measurement. Color Doppler images were obtained at a center frequency of 4.4 MHz and a pulse repetition frequency of 4 kHz (see Fig. 1). The Doppler velocity V of an arbitrary point is determined from the intensity of color, red for positive velocity and blue for negative velocity digitized into 256 grades using the color bar at upper right of Fig. 1.

For computation, we use grid C, which is twice as fine in each direction as grid B of the former section in order to depict the blood vessel shape in detail. The monitoring points are set at the grid points in the white rectangle in Fig. 11. The total number of the monitoring points is 864 with 36×24 points in each direction. In Fig. 1, the rectangle, where the monitoring points are placed, consists of 141×93 pixels. The time step of UMI simulation is determined as $\Delta t = 0.033$ s since the measurement data is obtained at that time interval. The uniform velocity profile is used at the upstream boundary condition. The residual at convergence is 1×10^{-5} and the maximum iteration number is 500. Two feedback formulae, A and B, are used in UMI simulation. Based on the result of the previous section, the gain K_v is determined as the maximum value which does not result in divergence of the computation. We performed UMI simulation using color Doppler images at the diagnosis of 6 cardiac cycles to obtain the final convergent solution. The timing when the maximum flow volume occurs in UMI simulation ($t = 0.23$ s) is designed to coincide with the measurement for synchronization.

Results and Discussion

The gains are determined as $K_v = 1.0$ for feedback A and $K_v = K_p = 0.2$ for feedback B after a number of trial computations. We are concerned here with the results in the final 6th cycle of UMI simulation and the corresponding ultrasound measurement, as well as that of the ordinary simulation in the 20th cycle in steady oscillation.

Figure 12 shows a comparison of the color Doppler images obtained by the color Doppler measurement, the ordinary simulation, and UMI simulations at $t = 0.38$ s in the deceleration phase as an example. The color Doppler image of the ordinary simulation is different from that of the measurement. The complicated mosaic pattern arising in the aneurysm in Fig. 12 (a) cannot be clearly seen in the ordinary simulation. In spite of the same condition as

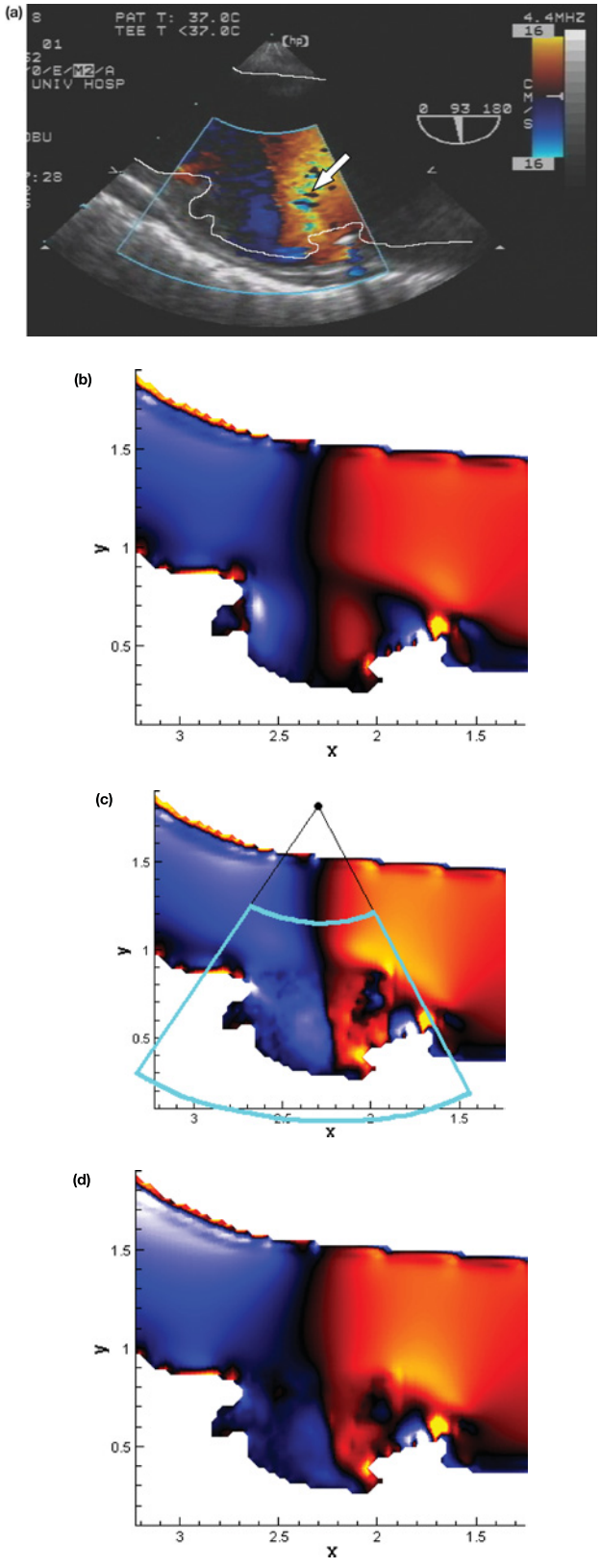

FIGURE 12. Comparison of color Doppler images at $t = 0.38$ s in deceleration phase among (a) real color Doppler image, (b) ordinary simulation, and (c) and (d) UMI simulations with feedback A and B of the real color Doppler data, respectively. Feedback A: $K_v = 1.0$, feedback B: $(K_v, K_p) = (0.2, 0.2)$.

TABLE 3. Comparison of average error norm of Doppler velocity.

	Average error norm $\bar{e}_{864}$
Ordinary simulation	1
UMI simulation	
Feedback A	0.483
Feedback B	0.511

the ordinary simulation except for the feedback, the color Doppler images of UMI simulations in Figs. 12(c) and (d) closely resemble that of the measurement including the mosaic pattern. We calculated average error norm $\bar{e}_{864}$ of Doppler velocity in the monitoring region as shown in Table 3. UMI simulation reduces the difference between the real color Doppler measurement and the ordinary simulation by a factor of 0.48 for feedback A or 0.51 for feedback B.

UMI simulation with feedback formula A reproduces the real measurement, including the aliasing [a white arrow in Fig. 12 (a)]. Here, aliasing indicated by a color different from the proper one occurs in the case in which the Doppler shift frequency exceeds one-half the pulse repetition frequency, which means that there is an excess of measurable maximum flow velocity and an incorrect result. Figure 13 shows the absolute value of the average instantaneous feedback intensity $|f_v|$ at each monitoring point viewed from the direction of the arrow in Fig. 11 for the same condition as Fig. 12. $|f_v|$ is the average absolute value of f_v during the iteration steps at a time step. In Fig. 13, the artificial force $|f_v|$ is large in the regions where the aliasing occurs (denoted with a white arrow) because large artificial forces are applied to compensate for the sudden velocity change due to aliasing. This means a peculiarly large feedback signal in UMI simulation can be used as an index of incorrect measurement such as aliasing. Improvement of UMI simulation using this information remains for future study.

By the first-order numerical differentiation of the computational result of the velocity component, the wall shear stress τ is calculated along the vessel wall with the aneurysm. Since the distribution of the wall shear stress shows an unnatural jagged shape because of the stepped-shape vessel wall defined by the orthogonal grid system, the result is smoothed by averaging five adjacent data points. Figures 14(a) and (b) show distribution of the time-averaged wall shear stress τ_{av} and the RMS value τ_{rms} of the wall shear stress in the aneurysm along the vessel wall measured from the upstream boundary as shown in Fig. 11. Comparison of those results reveals that a substantial difference exists between the results of time-averaged wall shear stress distributions but not those of the RMS values. The results of UMI simulations are probably better than that of the ordinary simulation. The wall shear stress is similar to that of the simulation with an aortic aneurysm by Finol and Amon.[4] However, we cannot say much about

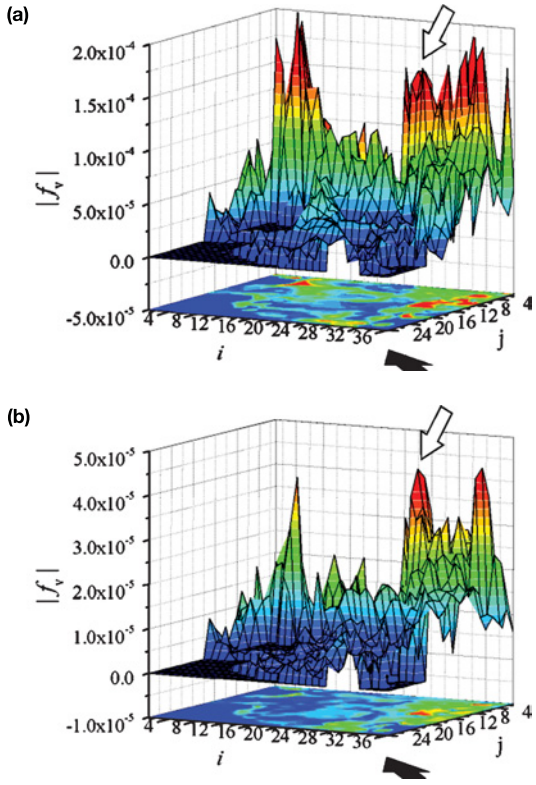

FIGURE 13. Average instantaneous feedback intensity with (a) feedback A and (b) feedback B at $t = 0.38$ s in deceleration phase (nondimensional).

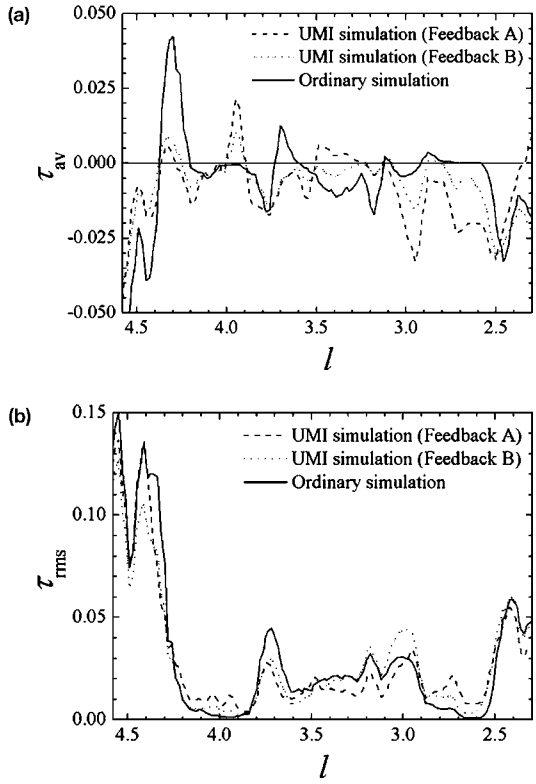

FIGURE 14. (a) Time-averaged wall shear stress τ_{av} and (b) RMS value τ_{rms} along the vessel wall (all results are nondimensional).

the validity of the results since there is no measurement data for the real wall shear stress distribution and the assumption of two-dimensionality limits the validity of the present model. Further research is needed, including three-dimensional analysis and verification by experiment.

CONCLUSIONS

In this paper we investigated fundamental characteristics of the Ultrasonic-Measurement-Integrated (UMI) simulation of blood flow in the aorta as a key issue to develop advanced medical diagnosis and treatment equipment. A UMI simulation was performed for a two-dimensional model problem using a standard numerical solution instead of the result of real ultrasonic measurement. Particularly, the effect of an incorrect upstream boundary velocity profile on the simulation result was investigated.

Results obtained in this study can be summarized as follows. For feedback formula A, by which artificial force is applied to the momentum equation to compensate for the error of the Doppler velocity between the numerical simulation and the standard solution, the error in velocity is significantly reduced in UMI simulation, but the error in pressure is intensified more than in the case of ordinary simulation. For feedback formula B, by which additional correction of the pressure equation is applied in feedback formula A, the error is reduced both in velocity and pressure in comparison with the ordinary simulation. Feedback B is more sensitive to the change of the feedback gain than feedback A.

Placement of the monitoring points in a partial domain effectively reduces the error in that part. UMI simulation requires additional computational time for feedback, but enhancement of convergence to the final solution results in a reduction of total computational time. Finally, UMI simulations with real color Doppler measurement were performed showing good agreement with the measurement.

The present study has confirmed the potential of UMI simulation for the reproduction of real blood flows by combining ultrasonic diagnostic equipment and a computer. It is essential to extend UMI simulation to three-dimensional problems and to perform complete verification theoretically, numerically, and experimentally in order to apply UMI simulation to the development of advanced medical diagnostic and treatment equipment.

ACKNOWLEDGMENTS

The computations were performed using the supercomputer system SGI ORIGIN 2000 in the Advanced Fluid Information Research Center, Institute of Fluid Science, Tohoku University. The authors are grateful to the staff of

the AFI Research Center for their support in the computational work.

REFERENCES

[1]Capineri, L., M. Scabia, and L. Masotti. A Doppler system for dynamic vector velocity maps. *Ultrasound Med. Biol.* 28:237–248, 2002.

[2]Caro, C. G., J. M. Fitz-Gerald, and R. C. Schroter. Atheroma and arterial wall shear. Observation, correlation and proposal of a shear dependent mass transfer mechanism for atherogenesis. *Proc. R. Soc. Lond. B Biol. Sci.* 117:109–159, 1971.

[3]Di Martino, E. S., G. Guadagni, A. Fumero, G. Ballerini, R. Spirito, P. Biglioli, and A. Redaelli. Fluid-structure interaction within realistic three-dimensional models of the aneurysmatic aorta as a guidance to assess the risk of rupture of the aneurysm. *Med. Eng. Phys.* 23:647–655, 2001.

[4]Finol, E. A., and C. H. Amon. Blood flow in abdominal aortic aneurysms: Pulsatile flow hemodynamics. *J. Biomech. Eng.* 123:474–484, 2001.

[5]Fletcher, C. A. J. *Computational Techniques for Fluid Dynamics*. Berlin: Springer-Verlag, 1988, pp. 302–303.

[6]Ganong, W. F. *Review of Medical Physiology*. 17th ed. Norwalk, CT: Appleton & Lange, 1995, 555 pp.

[7]Giddens, D. P., C. K. Zarins, and S. Glagov. The role of fluid mechanics in the localization and detection of atherosclerosis. *J. Biomech. Eng.* 115:588–594, 1993.

[8]Glor, F. P., J. J. M. Westenberg, J. Vierendeels, M. Danilouchkine, and P. Verdonck. Validation of the coupling of magnetic resonance imaging velocity measurements with computational fluid dynamics in a U bend. *Artif. Organs* 26:622–635, 2002.

[9]Hayase, T., and S. Hayashi. State estimator of flow as an integrated computational method with the feedback of online experimental measurement. *J. Fluids Eng.* 119:814–822, 1997.

[10]Hayase, T., J. A. C. Humphrey, and R. Greif. Mini-manual for ROTFLO2, Department of Mechanical Engineering Report FM-90-1, University of California, Berkeley, 1990.

[11]Hayase, T., J. A. C. Humphrey, and R. Greif. A consistently formulated QUICK scheme for fast and stable convergence using finite-volume iterative calculation procedures. *J. Comput. Phys.* 98:108–118, 1992.

[12]Jin, S., J. Oshinski, and D. P. Giddens. Effects of wall motion and compliance on flow patterns in the ascending aorta. *J. Biomech. Eng.* 125:347–354, 2003.

[13]Kilner, P. J., G. Z. Yang, R. H. Mohiaddin, D. N. Firmin, and D. B. Longmore. Helical and retrograde secondary flow patterns in the aortic arch studied by three-directional magnetic resonance velocity mapping. *Circulation* 88:2235–2247, 1993.

[14]Ku, D. N., D. P. Giddens, C. K. Zarins, and S. Glagov. Pulsatile flow and atherosclerosis in the human carotid bifurcation—positive correlation between plaque location and low and oscillating shear stress. *Atherosclerosis* 5:293–302, 1985.

[15]Liu, Y., Y. Lai, A. Nagaraj, B. Kane, A. Hamilton, R. Greene, D. D. McPherson, and K. B. Chandran. Pulsatile flow simulation in arterial vascular segments with intravascular ultrasound images. *Med. Eng. Phys.* 23:583–595, 2001.

[16]Nakamura, M., S. Wada, D. Mori, K. Tsubota, and T. Yamaguchi. Computational fluid dynamics study of the effect of the left ventricular flow ejection on the intraaortic flow. *Proc. AP Biomech. 2005* 61–62, 2004.

[17]Nisugi, K., T. Hayase, and A. Shirai. Fundamental study of hybrid wind tunnel integrating numerical simulation and experiment in analysis of flow field. *JSME Int. J. Ser. B* 47:593–604, 2004.

[18]Ohtsuki, S., and M. Tanaka. Doppler pressure field deduced from the Doppler velocity field in an observation plane in a fluid. *Ultrasound Med. Biol.* 29:1431–1438, 2003.

[19]Olufsen, M. S., C. S. Peskin, W. Y. Kim, E. M. Pedersen, A. Nadim, and J. Larsen. Numerical simulation and experimental validation of blood flow in arteries with structured-tree outflow conditions. *Ann. Biomed. Eng.* 28:1281–1299, 2000.

[20]Patankar, S. V. Numerical Heat Transfer and Fluid Flow. Washington, DC: Hemisphere, 1980.

[21]Sakas, G. Trends in medical imaging: From 2D to 3D. *Comput. Graph.* 26:577–587, 2002.

[22]Schmid-Schönbein, G. W. Biomechanics of microcirculatory blood perfusion. *Annu. Rev. Biomed. Eng.* 1:73–102, 1999.

[23]Schneider, G. E., and M. Zedan. A modified strongly implicit procedure for the numerical solution of field problems. *Numer. Heat Transfer* 4:1–19, 1981.

[24]Steinman, D. A. Image-based computational fluid dynamics modeling in realistic arterial geometries. *Ann. Biomed. Eng.* 30:483–497, 2002.

[25]Tateshima, S., Y. Murayama, J. P. Villablanca, T. Morino, H. Takahashi, T. Yamaguchi, K. Tanishita, and F. Viñuela. Intraaneurysmal flow dynamics study featuring an acrylic aneurysm model manufactured using a computerized tomography angiogram as a mold. *J. Neurosurg.* 95:1020–1027, 2001.

[26]Taylor, T. W., and T. Yamaguchi. Three-dimensional simulation of blood flow in an abdominal aortic aneurysm—steady and unsteady flow cases. *J. Biomech. Eng.* 116:89–97, 1994.

[27]The International Study of Unruptured Intracranial Aneurysms Investigators. Unruptured intracranial aneurysms—risk of rupture and risks of surgical intervention. *N. Engl. J. Med.* 339:1725–1733, 1998.

[28]Tortoli, P., G. Bambi, F. Guidi, and R. Muchada. Toward a better quantitative measurement of aortic flow. *Ultrasound Med. Biol.* 28:249–257, 2002.

[29]Ujiie, H., Y. Tamano, K. Sasaki, and T. Hori. Is the aspect ratio a reliable index for predicting the rupture of a saccular aneurysm? *Neurosurgery* 48:495–503, 2001.

[30]Zhao, S. Z., P. Papathanasopoulou, Q. Long, I. Marshall, and X. Y. Xu. Comparative study of magnetic resonance imaging and image-based computational fluid dynamics for quantification of pulsatile flow in a carotid bifurcation phantom. *Ann. Biomed. Eng.* 31:962–971, 2003.